Solar and Stellar Flares and their Effects on Planets
Proceedings IAU Symposium No. 320, 2015
A.G. Kosovichev, S.L. Hawley & P. Heinzel, eds.

doi:10.1017/S1743921316000302

High-temperature solar flare plasma behaviour from crystal spectrometer observations

Barbara Sylwester[1], Janusz Sylwester[1], Kenneth J.H. Phillips[2], Anna Kepa[1] and Tomasz Mrozek[1,3]

[1]Space Research Centre, Polish Academy of Sciences, Wrocław, Poland
email: bs@cbk.pan.wroc.pl

[2]Dept. of Earth Sciences, Natural History Museum, London SW7 5BD, U.K.
email: kennethjhphillips@yahoo.com

[3]Astronomical Institute of Wrocław University, Wrocław, Poland
email: mrozek@astro.uni.wroc.pl

Abstract. We present results of analysis of the spectra collected with Polish instrument RESIK flown on *CORONAS-F* satellite. RESIK was the bent crystal spectrometer, measuring spectra in the spectral range 3.3 - 6.1 Å with a high cadence during flares. The emission lines as well as the continuum observed by RESIK are formed in hotter ($T > 3$ MK) plasmas of active regions and flares. RESIK observed various types of flares: from X-ray class B and C up to strongest flares of X-class, for both, short and long duration events. The analysis of absolute and relative spectral intensities of the lines and continuum observed for 33 events allowed for determining the plasma elemental composition with subsequent detailed study of time changes of the temperature structure of the sources described in terms of the differential emission measure (DEM). As an example we present the typical DEM evolutionary patterns for the C1.9 flare (SOL2002-12-26T08:35) and discuss its thermodynamics.

Keywords. Sun: abundances, Sun: flares, Sun: X-rays

1. Introduction

In this contribution, we describe an analysis of X-ray spectra from the RESIK Bragg crystal spectrometer on *CORONAS-F* which was operational from 2001–2003. The RESIK X-ray spectrometer consisted of four channels in the 3.3 - 6.1 Å range, with bent crystals and positional-sensitive proportional counters. The instrument is described by Sylwester *et al.* (2005). The analysis uses a multi-temperature approach by taking the fluxes in narrow spectral intervals in RESIK spectra during thirty-three flares, and uses the Withbroe-Sylwester technique to obtain optimum element abundances for the spectral lines observed and temperature-dependent (differential) emission measure as a function of time. We find that in general the flare emission seen by RESIK consists of a high-temperature ("hot") and lower-temperature ("cool") component throughout the evolution of each flare. From images obtained with the *Reuven Ramaty High Energy Solar Spectroscopic Imager* (*RHESSI*: Lin *et al.* 2003), we obtain flare emitting volumes and lower limits to the electron densities. The time evolution of densities is derived for all the flares analyzed; here we summarize the analysis for one particular flare.

Table 1. Wavelength intervals used in this analysis

Number	Wavelength interval (Å)	RESIK Channel	Features in range
1	3.40 - 3.50	1	continuum
2	3.50 - 3.60	1	K XVIII lines + sat.
3	3.60 - 3.80	1	continuum
4	3.92 - 4.02	2	Ar XVII lines + sat.
5	4.11 - 4.17	2	continuum
6	4.17 - 4.21	2	S XV $1s^2 - 1s4p$ sat.
7	4.21 - 4.25	2	continuum
8	4.36 - 4.42	3	S XV d3 sat.
9	4.42 - 4.68	3	continuum
10	4.70 - 4.75	3	S XVI Lyα line
11	4.75 - 4.80	3	S XV sats to S XVI Lyα
12	5.00 - 5.15	4	S XV triplet + sat.
13	5.25 - 5.32	4	Si XIII $1s^2 - 1s5p$ line
14	5.37 - 5.48	4	Si XIII $1s^2 - 1s4p + 5p$ sat.
15	5.48 - 5.62	4	Si XII $4p$ sat.
16	5.64 - 5.71	4	Si XIII $1s^2 - 1s3p$ line
17	5.77 - 5.86	4	Si XII $3p$ sat.
18	5.92 - 5.97	4	continuum

2. RESIK data

The spectral range of RESIK includes resonance and other emission lines due to highly ionized potassium (K XVIII), argon (Ar XVII), sulphur (S XV, S XVI), and silicon (Si XIII, Si XIV), with a number of dielectronic satellite line features such as those due to Si XII. For large flares Cl XVII lines are also evident though very weak. Continuum emission is observed in the two low-wavelength channels (1 and 2), covering 3.40 - 4.27 Å, but an instrumental background, due to crystal fluorescence, contributes to the emission in channels 3 and 4 (4.35 - 6.05 Å). RESIK was an uncollimated spectrometer, so that slightly different wavelength ranges were obtained for flare emission off-axis.

Table 1 lists 18 spectral intervals containing both emission lines and apparently line-free ("continuum") emission. The wavelength range of each interval is given in Col. 2, and the RESIK channel number is indicated (Col. 3). Line identification is given in Col. 4. "Sat." indicates a dielectronic satellite feature (generally a group of satellite lines forming a single, unresolved line feature). In Figure 1 the corresponding normalized emission functions for selected wavebands are presented. Emission functions were calculated using the CHIANTI 7.1 code.

3. Analysis: Element Abundances

Our object is to obtain differential emission measure (DEM) from the fluxes in the spectral intervals listed in Table 1. With $\mathfrak{F}_i$ the flux in spectral interval i and $G(T_e)$ the emission function (i.e. the amount of emission seen at Earth distance from an emitting volume of 1 cm^3 in the solar corona at electron temperature T_e), the DEM is solved from an integral equation:

$$\mathfrak{F}_i = Ab_i \int_{T_e=0}^{\infty} G_i(T_e) DEM(T_e) dT_e \qquad (3.1)$$

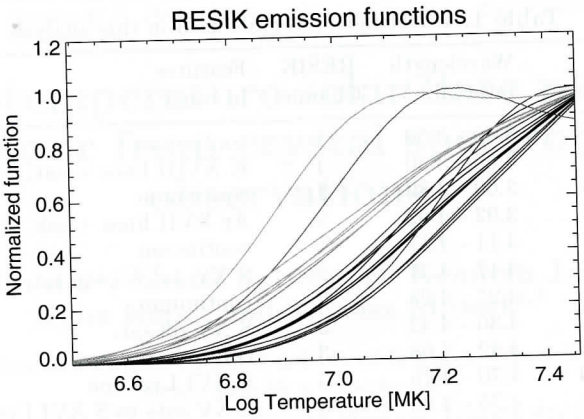

Figure 1. The temperature behaviour of normalized emission functions for 18 wavebands used in the analysis (see Table 1). Emission functions were calculated using CHIANTI 7.1 code.

where Ab_i is the abundance of the element that contributes to the spectral interval (either a spectral line or the free–bound continuum). In terms of emitting volume V, electron density N_e and T_e, DEM is defined by

$$DEM = N_e^2 \frac{dV}{dT_e}. \tag{3.2}$$

The solution of DEM is well known to be ill-conditioned, as shown by various authors (e.g. Craig & Brown 1976), but methods exist in which the DEM satisfies the input fluxes within uncertainties and has physical meaning. Our method has been the Withbroe–Sylwester method, as described by Sylwester & Sylwester (1999), which has been used extensively by us in the past. We have tested the method on synthetic data and assumed DEM functional forms, and the DEMs have been successfully recovered after the inversion.

In a first step of the analysis, the element abundances are given first-guess values which are coronal values as given, e.g., by Feldman *et al.* (1992). Theory spectra covering the RESIK ranges are generated every time and the quality of the fit is noted after 1000 iterations. Plots are then constructed showing the dependence of the fit quality, measured by χ^2, on element abundance. For the elements with strong contributions to the RESIK spectra, well-defined minima in χ^2 are apparent, which are then taken to be the element abundance in the second step analysis. The uncertainties in the abundance estimate, given by values corresponding to $\min(\chi^2) + 1$, are noted also.

We took a total of 33 flares observed by RESIK, both on the solar disk and near the limb. The X-ray classes ranged from B9.9 to X (an X1.5 flare, partially observed - the rise and decay phases only). Some 26 flares had X-ray class between C1 and C9, five of class M. The derived abundances from this first step in the analysis have been published (Sylwester *et al.* 2014); to summarize, they are (on a logarithmic scale with H=12): Ab(K) $= 5.73 \pm 0.19$, Ab(Ar) $= 6.47 \pm 0.08$, Ab(S) $= 6.91 \pm 0.07$ (always slightly below photospheric), and Ab(Si) $= 7.53 \pm 0.08$ (approximately equal to photospheric). These estimates may be compared with our previous estimates from an isothermal analysis: for K and Ar, they are very similar, but are significantly lower for S and Si. Further details are given by Sylwester *et al.* 2014. Note that for Ar, our present (and previous) estimate is

very similar to that derived by Lodders (2008), and for K, the abundance is much higher than is indicated by Feldman *et al.* (1992). Our results differ from the much-discussed FIP picture (FIP = First Ionization Potential), in which elements with low (< 10 eV) FIP have enhanced coronal abundances but elements with high FIP (10 eV or more) are equal to photospheric abundances (e.g. Asplund *et al.* 2009).

4. Differential Emission Measure

The derivation of differential emission measure DEM is described in an earlier work (Sylwester *et al.* (2014)) so we will give only a brief outline here. The element abundances for K, Ar, S, and Si were taken from the procedure already described, while the abundances of other elements were taken from Feldman *et al.* (1992). Ion fractions were taken from Bryans *et al.* (2009). The Withbroe-Sylwester procedure was then used for inversion of Equation 3.1 to find DEM, with convergence continued to iteration 10000. Uncertainties were derived from Monte Carlo runs, in which input values of $\mathfrak{F}_i$ were given random perturbations with statistical uncertainties.

Figure 2 shows the results of this inversion for a C1.9 limb flare occurring on December 26, 2002 (SOL2002-12-26T08:35). The top left-hand panel shows the DEM solution as a time and temperature plot, with time (in minutes) advancing upwards from 08:25:40 UT. As is very typical of the 33 flares we analyzed, a hotter and a cooler component of the DEM are evident (towards right and left of the yellow dashed line in the Figure), particular during the flare rise and peak stages. The centre upper panel shows the values of the total emission measure in each component as a function of time. The cooler (black) component has a total emission measure that is a factor of 100 larger than the hotter component (red). An emission measure can be evaluated from the ratio of the fluxes in the two channels of *GOES*: this is shown as the blue curve in the panel. As is generally the case, the *GOES* emission measure is intermediate between those of the hotter and cooler components. The centre lower panel shows the ratio of emission measures in the hotter and cooler components. Note that the components viewed by RESIK refer to the total flare emission as RESIK is an uncollimated instrument.

Very rough estimates of electron density may be made by comparing the total emission measure in the hot component with the area (Figure 2, upper right panel), and by assumption of a spherical volume, the volume of the hard X-ray emission as observed by *RHESSI* images constructed from the PIXON routine. These are given as a function of time in Figure 2, lower right panel. As can be seen, these are somewhat lower than what are generally accepted for flare densities (see e.g. Milligan *et al.* 2012). This probably reflects the neglect of unresolved fine structure in the *RHESSI* images.

5. Conclusions

This analysis of thirty-three flares observed by the RESIK instrument on *CORONAS-F* near the peak of the last solar cycle indicates that the X-ray emission arises from basically two separate components, a cooler (temperature $3 - 9$ MK) and a hotter component (temperature > 9 MK), the latter particularly evident in the rise and peak stages of each flare. This typical pattern indicates a near-universality of this behaviour. Lower limits to electron density N_e are estimated from the emission measure of the hot component and the volume as determined based on PIXON-reconstructed flare images from *RHESSI*. The initial step in the analysis gives element abundances which differ from what has become a standard picture of the FIP dependence of coronal abundances, in particular K is much more abundant than that indicated by Feldman *et al.* (1992), Si and S are

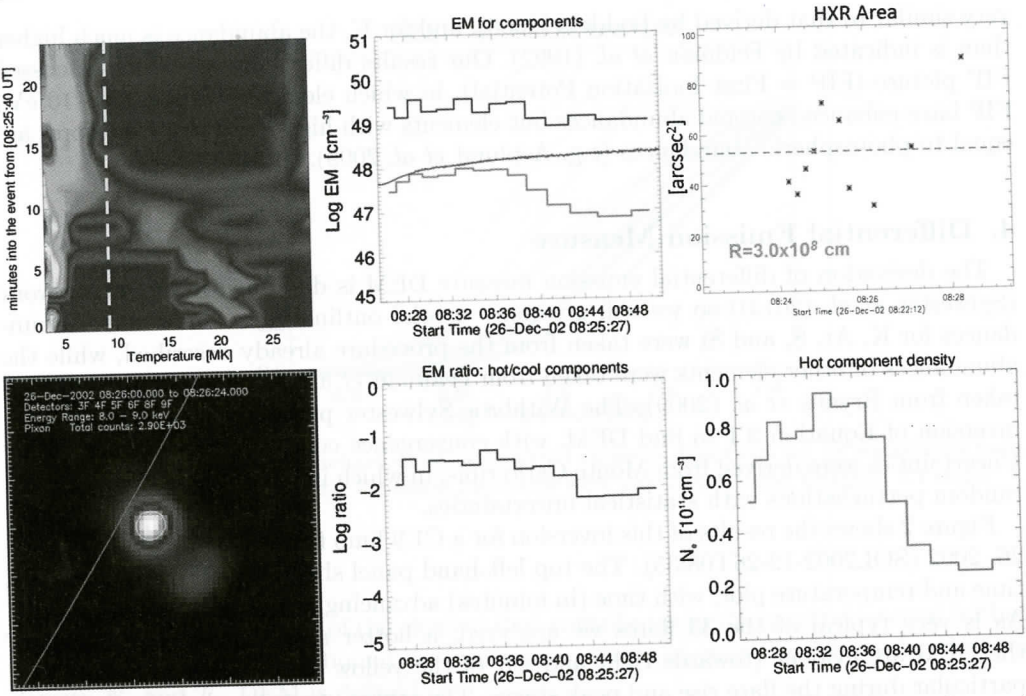

Figure 2. Results of the DEM analysis of the C1.9 limb flare on December 26, 2002 observed by RESIK. Top panels: (left) differential emission measure as a time and temperature plot, time proceeding upwards in minutes from 08:25:40 UT, yellow dashed line divides into cooler and hotter regions; (centre) total emission measures in the hotter (red) and cooler (black) components (blue line is the emission measure from the ratio of the two *GOES* channels); (right) hard X-ray area as estimated from *RHESSI* images as a function of time. Lower panels: *RHESSI* image in the 8-9 keV range at the start of the flare, limb shown as the yellow line; (centre) ratio of the hotter to cooler component emission measures as a function of time; (right) estimated electron densities from the total emission measure in the hotter component and the emission volume from *RHESSI* images.

nearly the photospheric abundances as given by Asplund *et al.* (2009). We are currently looking at possible scaling laws that would allow the estimate of the hotter component density and the total energy and duration of flares.

Acknowledgements

We acknowledge financial support from the Polish National Science Centre grant number 2011/01/M/ST9/06096 and UMO-2013-11/B/ST9/00234.

References

Asplund, M., Grevesse, N., Sauval, A. J., & Scott, P. 2009, *ARAA*, 47, 481
Bryans, P., Landi, E., & Savin, D. W. 2009, *ApJ*, 691, 1540
Craig, I. J. D. & Brown, J. C. 1976, *A&A*, 49, 239
Feldman, U., Mandelbaum, P., Seely, J. F., Doschek, G. A., & Gursky, H. 1992, *ApJS*, 81, 387
Lin, R. P. *et al.* 2003, *Sol. Phys.*, 210, 3
Lodders 2008, *ApJ*, 674, 607

Milligan, R. O., Kennedy, M. B., Mathioudakis, M., & Keenan, F. P. 2012, *ApJL*, 755, 16
Sylwester, B., Sylwester, J., Phillips, K. J. H., Kepa, A., & Mrozek, T. 2014 *ApJ*, 787, 122
Sylwester, B., Sylwester, J., Phillips, K. J. H., Kepa, A., & Mrozek, T. 2015 *ApJ*, 805, 49
Sylwester, J. & Sylwester, B. 1999, *Acta Astr.*, 49, 189
Sylwester, J., *et al.* 2005, *Sol. Phys.*, 226, 45